nature climate change

SUPPLEMENTARY INFORMATION

https://doi.org/10.1038/s41558-018-0140-y

In the format provided by the authors and unedited.

Increasing precipitation volatility in twenty-first-century California

Daniel L. Swain[1,2]*, Baird Langenbrunner[3,4], J. David Neelin[3] and Alex Hall[3]

[1]Institute of the Environment and Sustainability, University of California, Los Angeles, Los Angeles, CA, USA. [2]The Nature Conservancy, Arlington, VA, USA. [3]Department of Atmospheric and Oceanic Sciences, University of California, Los Angeles, Los Angeles, CA, USA. [4]Department of Earth System Science, University of California, Irvine, Irvine, CA, USA. *e-mail: dlswain@ucla.edu

Increasing precipitation volatility in 21st century California

Daniel L. Swain, Baird Langenbrunner, J. David Neelin, Alex Hall

Figure S1

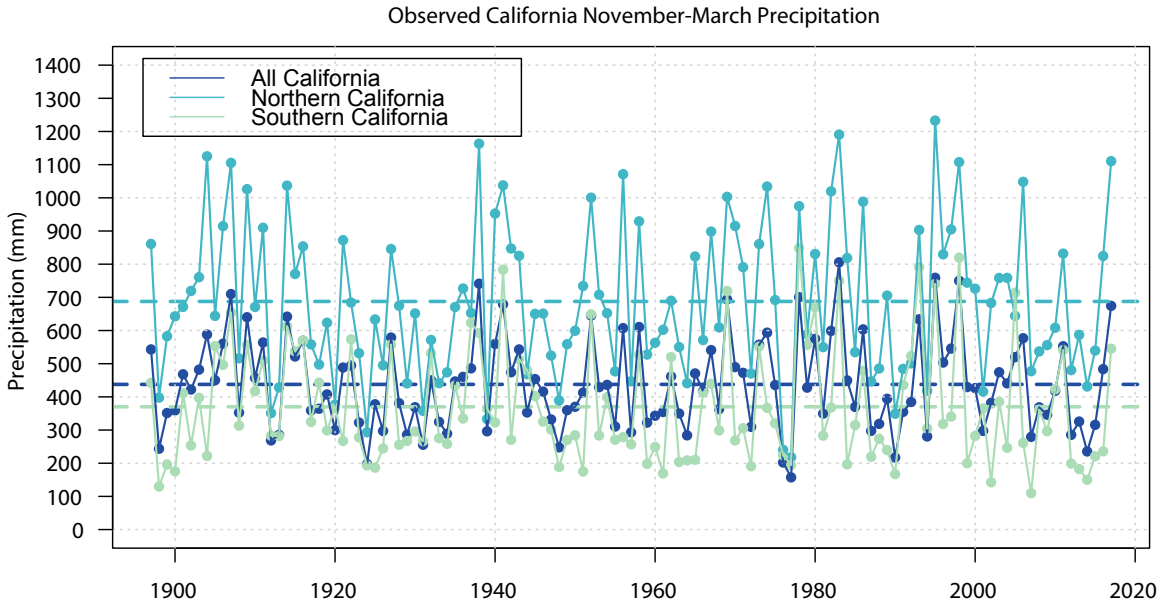

Figure S1 caption: Observed seasonal precipitation in California, 1895-2017. November – March mean seasonal precipitation for the full state of California (dark blue), northern California (light blue), and southern California (light green). Data from NOAA/NCDC nClimDiv dataset.

Figure S2

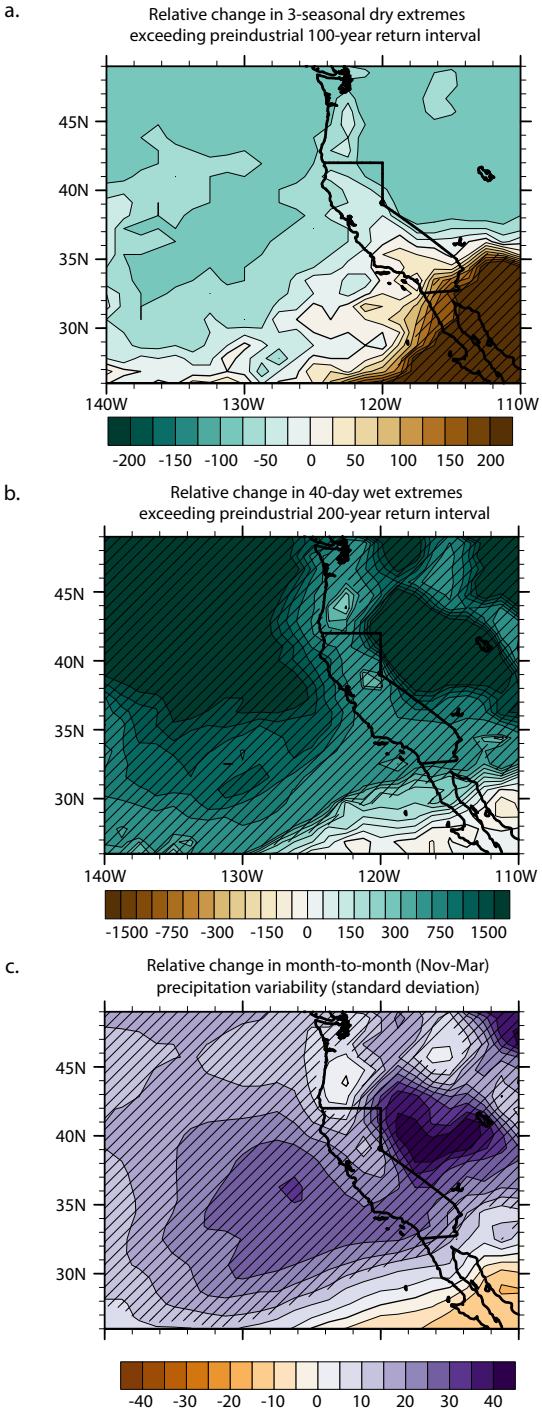
a.
Relative change in 3-seasonal dry extremes
exceeding preindustrial 100-year return interval
45N
40N
35N
30N
140W
130W
120W
110W
-200 -150 -100 -50 0 50 100 150 200
b.
Relative change in 40-day wet extremes
exceeding preindustrial 200-year return interval
45N
40N
35N
30N
140W
130W
120W
110W
-1500 -750 -300 -150 0 150 300 750 1500
c.
Relative change in month-to-month (Nov-Mar)
precipitation variability (standard deviation)
45N
40N
35N
30N
-40 -30 -20 -10 0 10 20 30 40

Figure S2 caption: Change in frequency of hydroclimatic extremes. a.) Relative (%) change in frequency of extremely dry 3-year periods (meeting or falling below the 100-year preindustrial return interval for November-March precipitation on a 3-year running mean basis) at end of 21st century (2070-2100, RCP8.5 forcing) relative to the preindustrial era (1850 forcing). Cross-hatching signifies 90% statistical confidence ($p < 0.10$) in robustness of frequency shifts across the full 40-member CESM-LENS ensemble. b.) Relative (%) change in frequency of extremely wet sub-seasonal storm sequences (meeting or exceeding the 200-year preindustrial return interval for cumulative 40-day precipitation) at end of 21st century (2070-2100, RCP8.5 forcing) relative to the preindustrial era (1850 forcing). Cross-hatching signifies 90% statistical confidence ($p < 0.10$) in robustness of frequency shifts across the full 40-member CESM-LENS ensemble. c.) Relative (%) change in the standard deviation of monthly precipitation during the November-March rainy season at end of 21st century (2070-2100, RCP8.5 forcing) relative to the preindustrial era (1850 forcing). Cross-hatching signifies 90% statistical confidence ($p < 0.10$) in robustness of frequency shifts across the full 40-member CESM-LENS ensemble.

Figure S3

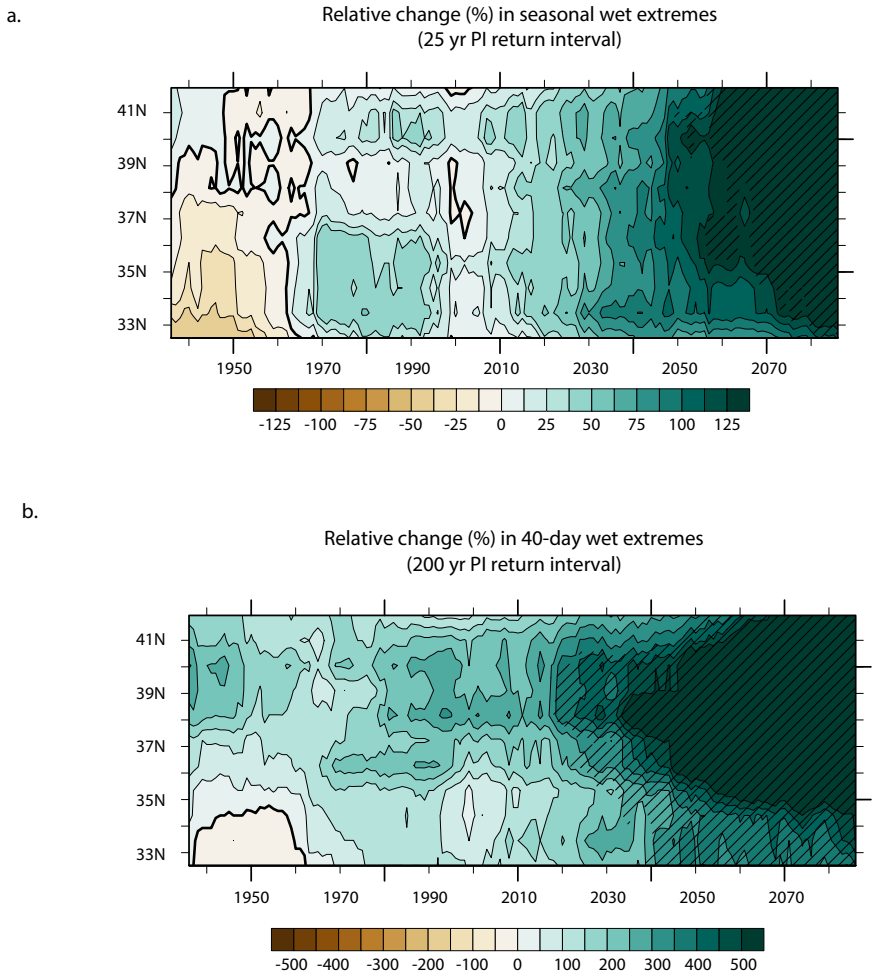

Figure S3 caption: Emergence of extreme wet event frequency shifts. a.) Time-latitude plot depicting evolution of frequency changes for extremely wet November-March seasons (25-year return interval) at different latitudes near California coast, temporally smoothed over 30-year intervals. b.) Same as (a.), but for extremely wet sub-subseasonal storm sequences (200-year return interval). Cross-hatching signifies 90% statistical confidence ($p < 0.10$) in robustness of frequency shifts across the full 40-member CESM-LENS ensemble.

Figure S4

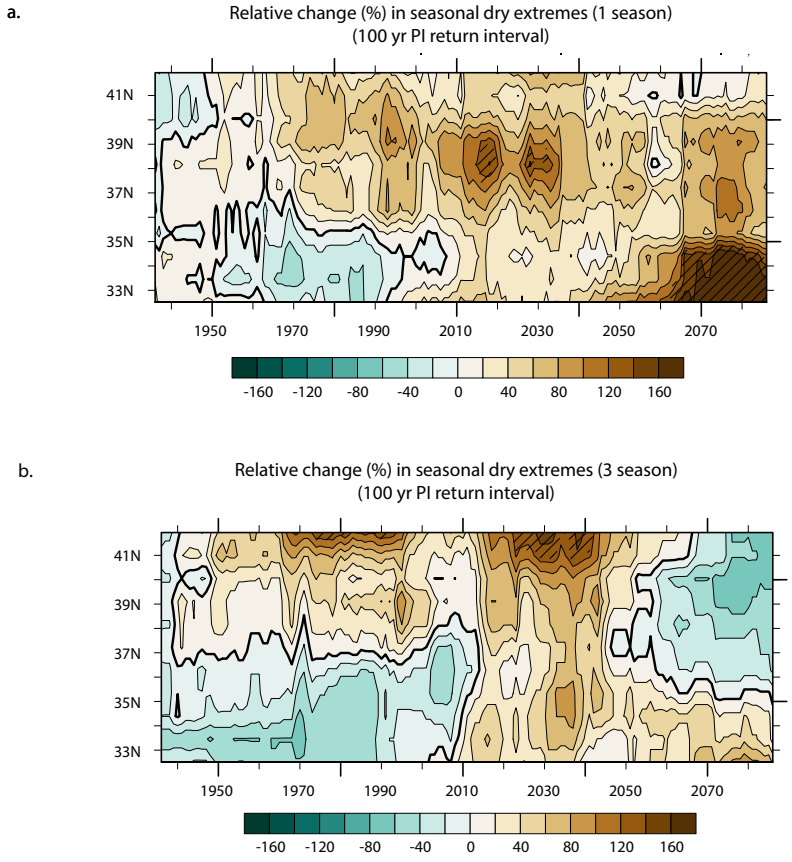

Figure S4 caption: Emergence of extreme dry event frequency shifts. a.) Time-latitude plot depicting evolution of frequency changes for extremely dry November-March seasons (100-year return interval) at different latitudes near California coast, temporally smoothed over 30-year intervals. b.) Same as (a.), but for extremely dry consecutive seasons (running 3-year mean of November-March precipitation, 100-year return interval). Cross-hatching signifies 90% statistical confidence ($p < 0.10$) in robustness of frequency shifts across the full 40-member CESM-LENS ensemble.

Figure S5

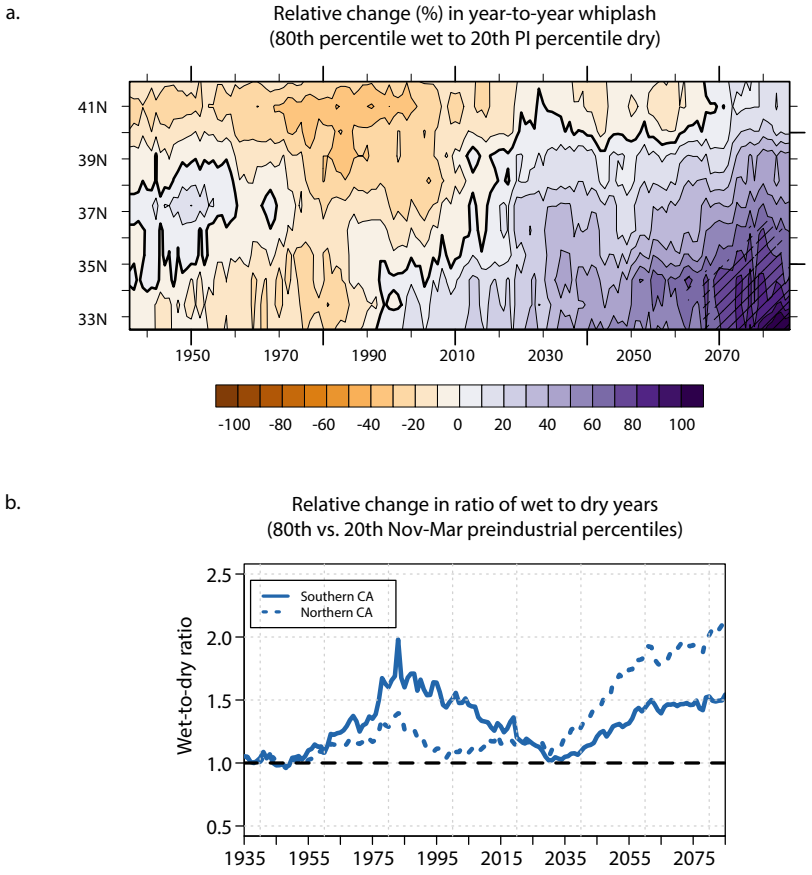

Figure S5 caption: Emergence of precipitation whiplash frequency shifts. a.) Time-latitude plot depicting evolution of frequency changes for wet-to-dry whiplash events at different latitudes near California coast, temporally smoothed over 30-year intervals. Cross-hatching signifies 90% statistical confidence ($p < 0.10$) in robustness of frequency shifts across the full 40-member CESM-LENS ensemble. b.) Ensemble mean ratio of occurrence of wet seasons (at or above 80th preindustrial percentile) to dry seasons (at or below 20th preindustrial percentile) between 1935 and 2085 for cluster of grid boxes centered in southern and northern California, respectively. Data are smoothed over 30-year intervals.

Figure S6

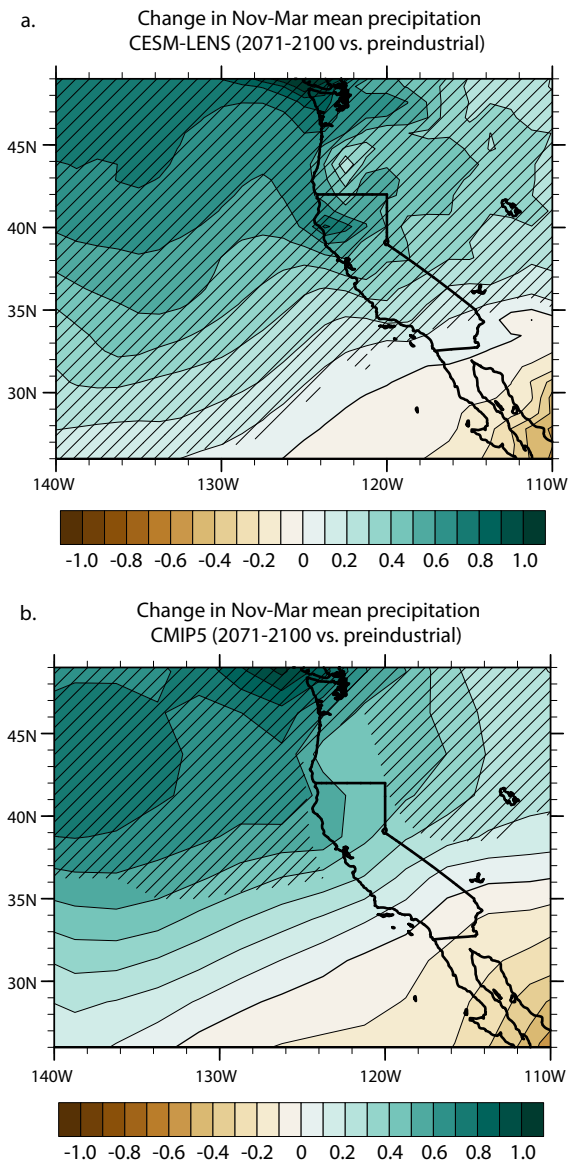

Figure S6 caption: Comparison of CESM-LENS vs. CMIP5 ensemble mean precipitation. a.) Simulated ensemble mean changes in seasonal mean November-March precipitation at end of 21st century (2070-2100) vs. the historical period (1920-2005) in CESM-LENS. b.) Same as (a.), but for the CMIP5 ensemble mean. In both plots, cross-hatching denotes regions where 2/3 of ensemble members agree on the sign of mean seasonal precipitation change.

Figure S7

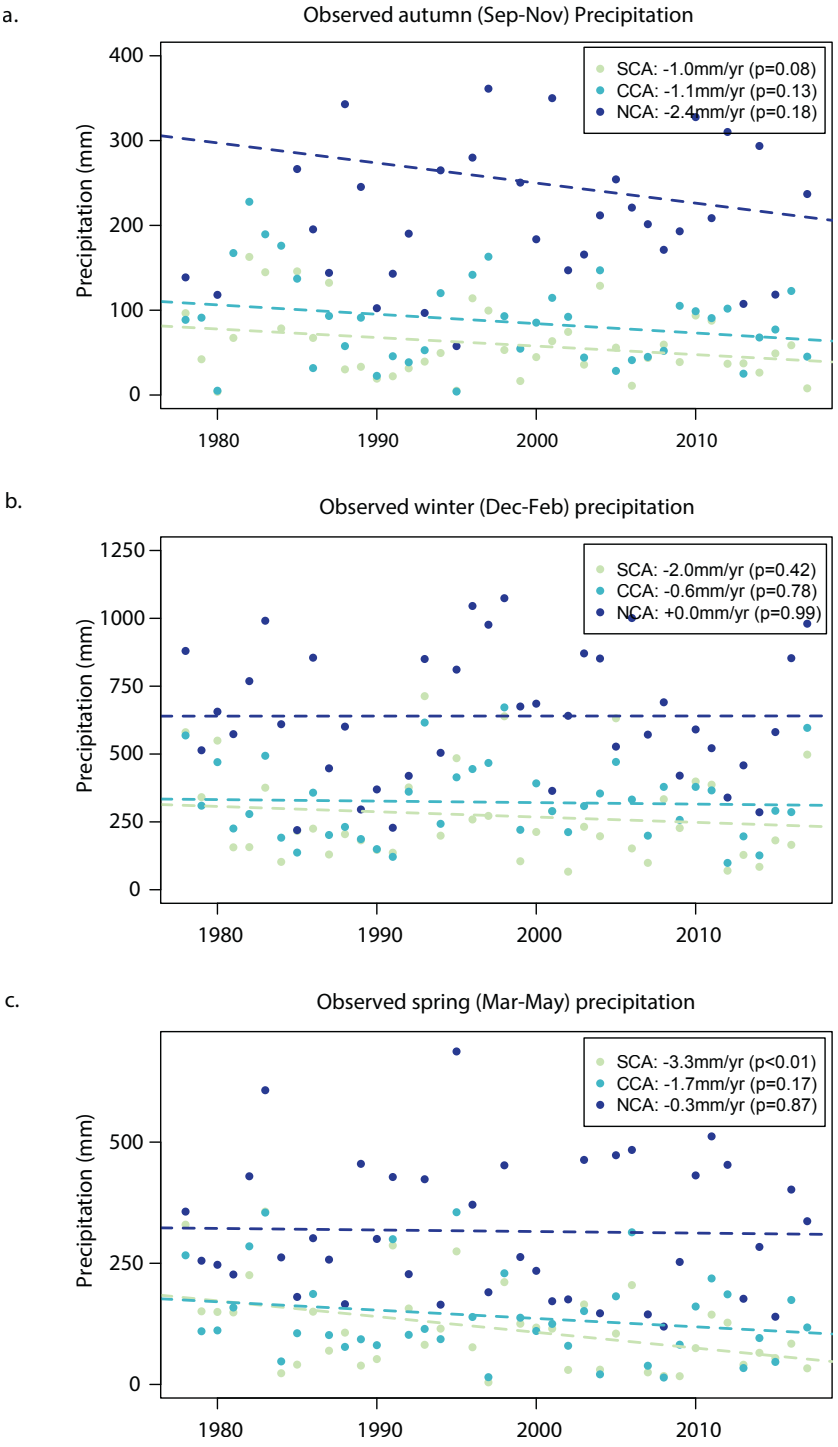
a.
Observed autumn (Sep-Nov) Precipitation
SCA: -1.0mm/yr (p=0.08)
CCA: -1.1mm/yr (p=0.13)
NCA: -2.4mm/yr (p=0.18)
Precipitation (mm)
0
100
200
300
400
1980
1990
2000
2010
b.
Observed winter (Dec-Feb) precipitation
SCA: -2.0mm/yr (p=0.42)
CCA: -0.6mm/yr (p=0.78)
NCA: +0.0mm/yr (p=0.99)
Precipitation (mm)
0
250
500
750
1000
1250
1980
1990
2000
2010
c.
Observed spring (Mar-May) precipitation
SCA: -3.3mm/yr (p<0.01)
CCA: -1.7mm/yr (p=0.17)
NCA: -0.3mm/yr (p=0.87)
Precipitation (mm)
0
250
500
1980
1990
2000
2010

Figure S7 caption: Observed changes in seasonality of California precipitation. Observed mean seasonal precipitation for three coastal California climate regions (dark blue=North Coast; light blue=Central Coast; light green=South Coast) for the most recent 40 year period (through autumn 2017). Data from NOAA/NCDC nClimDiv dataset. P-values denote statistical significance of mean linear trend within each climate region and season using a standard two-tailed test.

Figure S8

a. 500mb GPH difference, RCP8.5 minus PIC (November-March climatology)

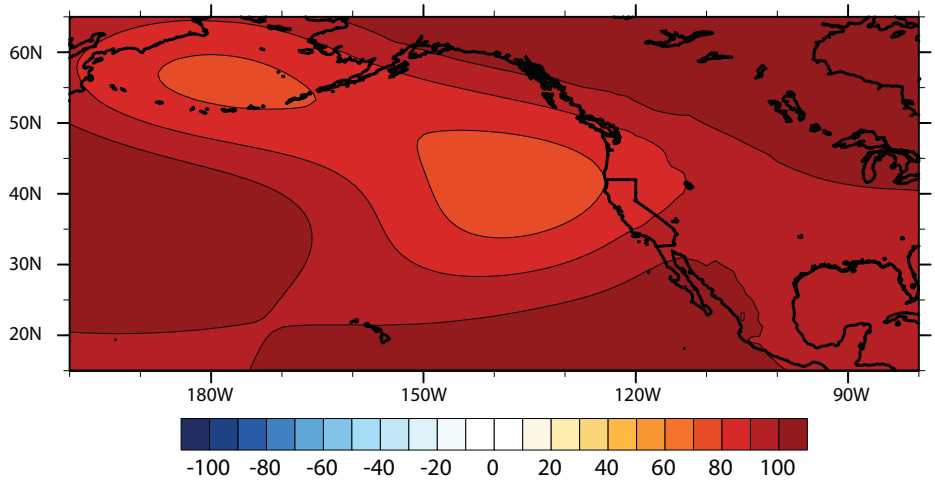

b. Vertically integrated Q difference, RCP8.5 minus PIC (November-March climatology)

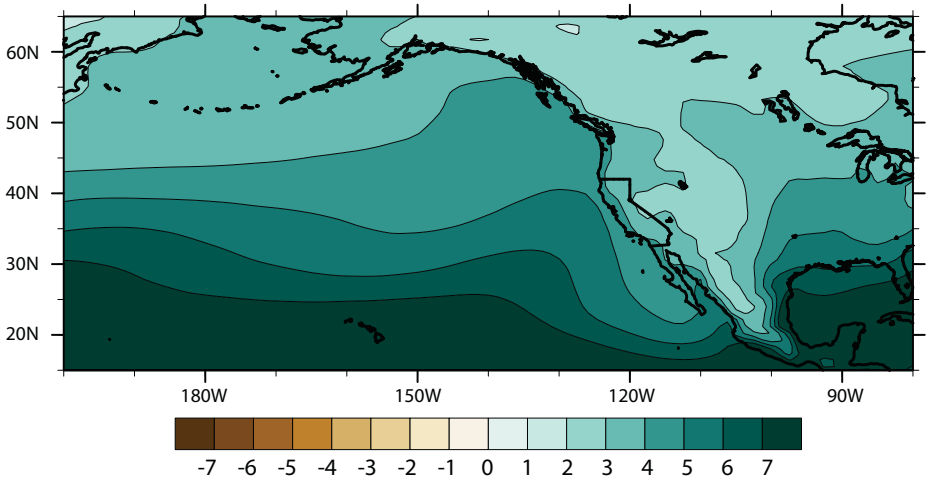

Figure S8 caption: Mean change in geopotential height and integrated water vapor, RCP8.5 vs. PIC. a.) Simulated mean change in November-March 500hPa geopotential height (GPH, meters) between RCP8.5 (2081-2100). b.) Same as (a.), but for vertically-integrated water vapor (Q, g kg^{-1})

Figure S9

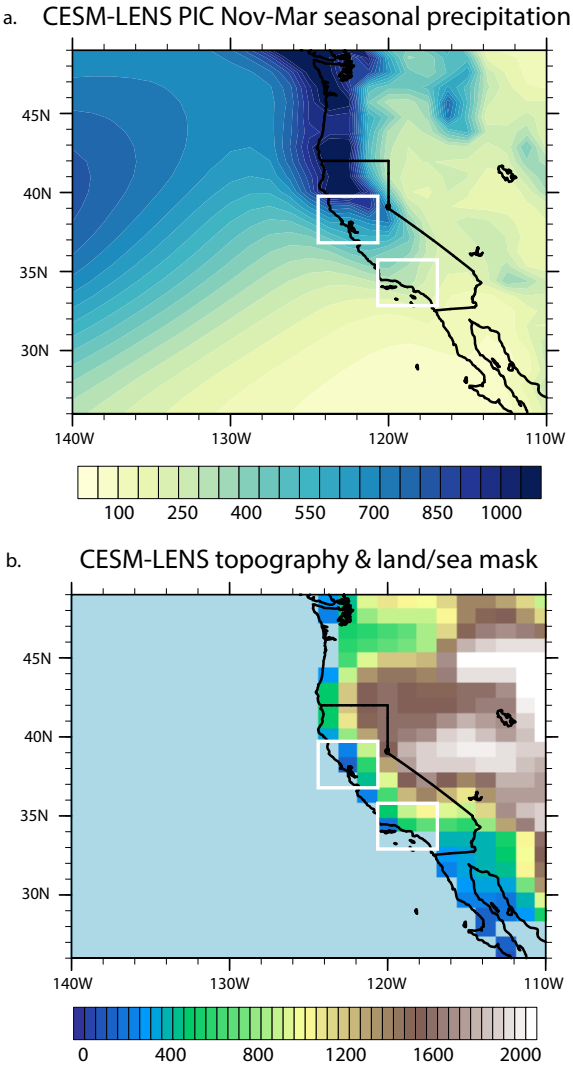

Figure S9 caption: CESM-LENS mean November-March precipitation in relation to model topography. a.) Mean March-November precipitation during the CESM-LENS PIC simulation. b.) Topography (derived from surface geopotential, meters) and land/sea mask (ocean shown as light blue shading; land shown as rasterized topography contours) provided as boundary conditions in CESM-LENS. White boxes in (a.) and (b.) denote 9-gridbox regions used to define "southern California" and "northern California" for the purposes of the time series presented in Figs. 1-4.

Figure S10

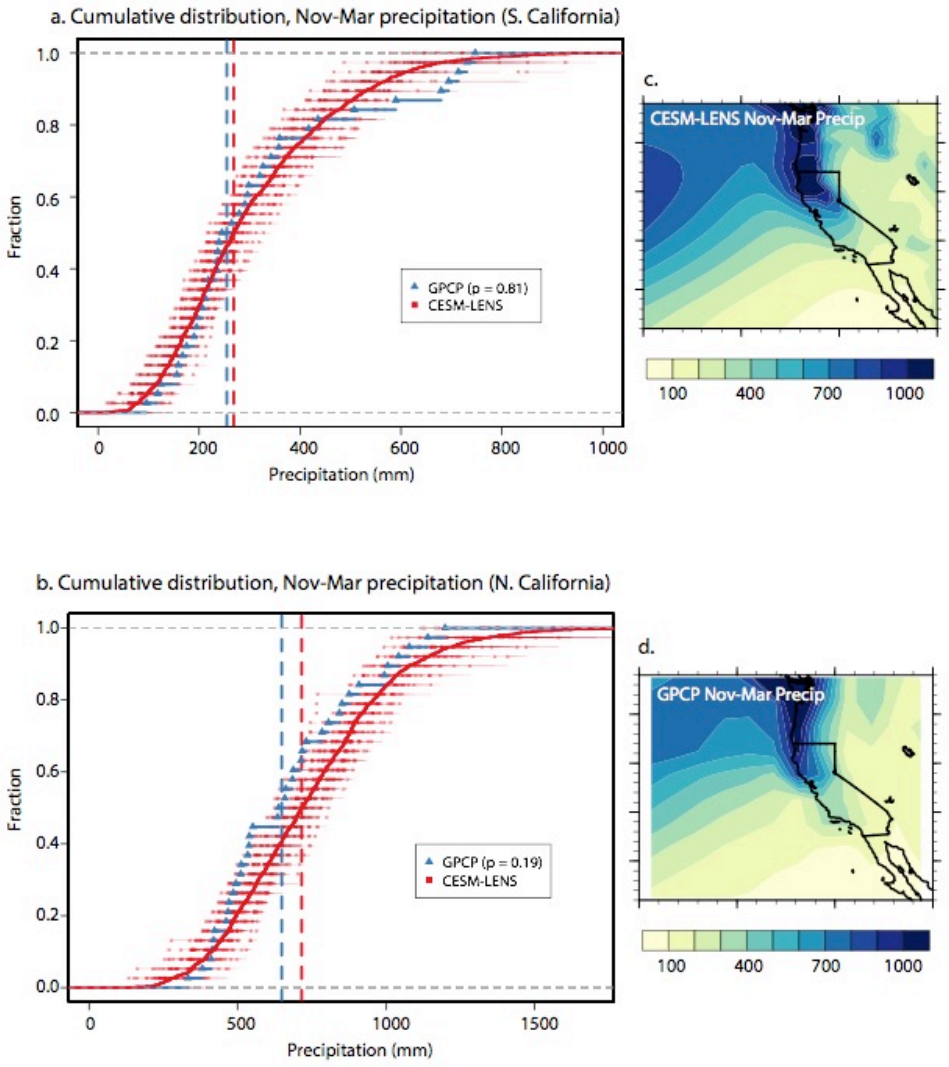

Figure S10 caption: Observational validation of CESM-LENS precipitation in California. Comparison of ensemble mean empirical cumulative distribution of CESM-LENS November-March seasonal precipitation distribution (solid red curve) to independent observational dataset (GPCP; blue triangles) across (a.) Southern California and (b.) Northern California for the 1980-

2016 period. In both panels, the dashed vertical lines correspond to the seasonal median precipitation for each dataset. In the panel legends, p-values correspond to the outcome of a Kolgoromov-Smirnoff (K-S) "sameness of distribution" test (p-values >0.05 suggest the distributions are not statistically distinguishable). c.) Map depicting CESM-LENS ensemble mean seasonal (November-March) seasonal precipitation. d.) Same as (c.), but for GPCP observations. Horizontal distributions of red squares in (a.) and b.) represent ensemble spread across the full 40 members of the CESM-LENS, with the empirical cumulative distribution from each realization plotted separately.

Figure S11

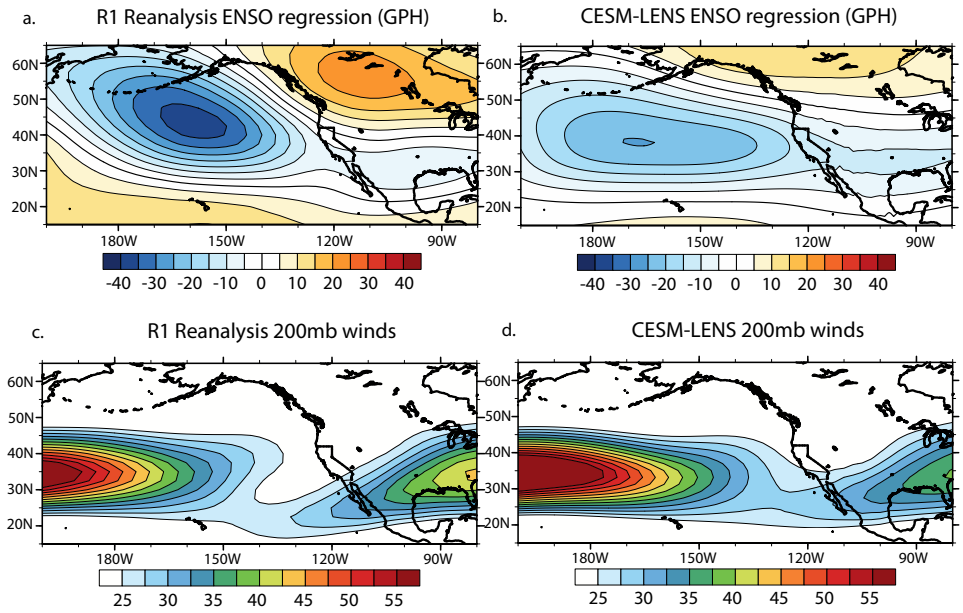

Figure S11 caption: Observed and simulated ENSO teleconnections and jet stream relationships. a.) Linear regression of 500hPa geopotential heights (GPH, meters) on Nino3.4 region sea surface temperatures (SST) using November-March data from R1 NCAR/NCEP reanalysis. b.) As in (a.) but for CESM-LENS during the preindustrial control simulation. c.) Strength of jet stream-level (200hPa) winds (m/s) during November-March using data from the R1 reanalysis (1950-2005). d.) Same as (c.), but for CESM-LENS during a subset of the historical period (1950-2005).

Figure S12

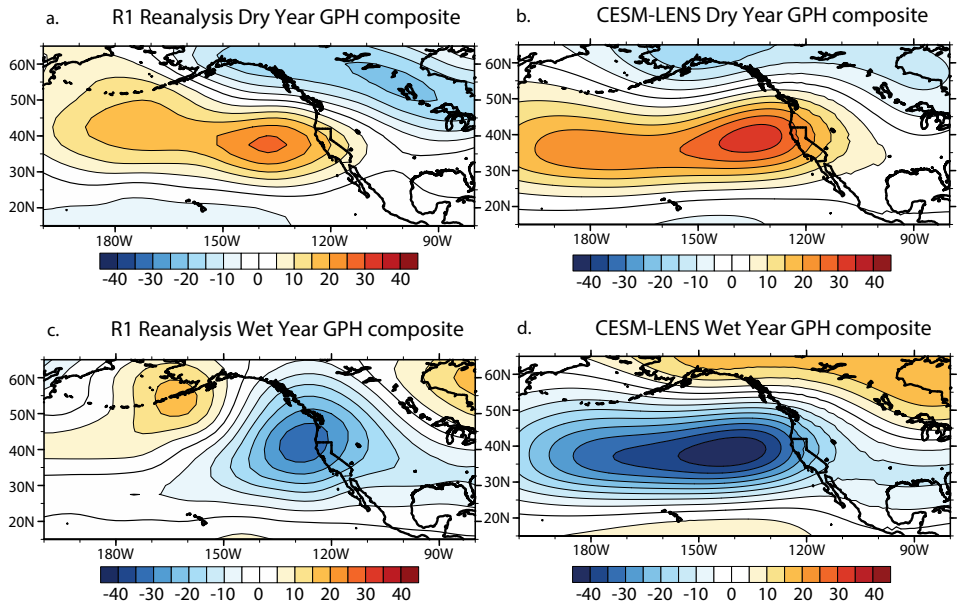

Figure S12 caption: Observed and simulated geopotential height composite maps during California dry and wet years. a.-d.) Composite maps depicting anomalies in November-March 500hPa geopotential height (GPH, meters) during wet (80th percentile, left column) and dry (20th percentile, right column) March-November seasons in the R1 NCEP/NCAR reanalysis (left column) and the CESM-LENS simulation (right column). Observed dry and wet California years are assessed using precipitation data from NOAA's nClimDiv divisional climate dataset during the interval that overlaps with the R1 dataset (1949-2017).